Spectroscopy Studies of Macrocyclic Supramolecular Assembly

41

Zixin Yang, Hao Tang, and Yu Liu

Contents

Z. Yang
College of Science, Huazhong Agricultural University, Wuhan, China
e-mail: zixinyang@mail.hzau.edu.cn

H. Tang
School of Chemistry and Chemical Engineering, South China University of Technology, Guangzhou, China
e-mail: haotang@scut.edu.cn

Y. Liu (✉)
College of Chemistry, State Key Laboratory of Elemento-Organic Chemistry, Nankai University, Tianjin, China

Collaborative Innovation Center of Chemical Science and Engineering (Tianjin), Tianjin, China
e-mail: yuliu@nankai.edu.cn

Y. Liu et al. (eds.), *Handbook of Macrocyclic Supramolecular Assembly*,
https://doi.org/10.1007/978-981-15-2686-2_47

41.1 Introduction

Supramolecular chemistry, which evolved from host-guest chemistry, has been prospering in many rapidly expanding fields, such as molecular machines and motors, molecular sensors, dynamic combinatorial chemistry, and supramolecular polymers [1]. In supramolecular systems, various building blocks are held together and organized by many simultaneous intermolecular forces and therefore generate new and exciting properties and functions that surpass those of the blocks. A supramolecular system is of structural complexity and dynamic reversibility, and thus detailed information on these aspects allows chemists to have a deep understanding of the relationship among the properties of supramolecular system, the underlying microstructure of assemblies and the molecular structure of the blocks [2]. Spectroscopies are important and effective methodologies to deeply reflect the molecular structure characteristics and various dynamic processes proceeded within and between molecules. As a result, they have been widely used in the study of supramolecular chemistry [3–7].

In this chapter, absorbance, fluorescence, NMR, and ICD spectroscopies in supramolecular chemistry are introduced. With practical examples, some fundamental and common techniques of these four spectroscopies are discussed. The chapter begins with absorbance and fluorescence spectroscopies, which are proven powerful tools to study the characteristics of supramolecular microenvironment as well as the supramolecular interaction between the building blocks. The ultraviolet-visible spectrophotometer and the spectrofluorophotometer are two of the most commonly used spectroscopic instruments in the laboratory. Therefore the basic principles of the experimental design and conduction, the qualitative and quantitative analysis are introduced in detailed. Next, 1D and 2D NMR spectroscopies including COSY, NOESY, ROESY, and DOSY are introduced as powerful techniques for the structure investigation. Then CD spectroscopy for supramolecular conformation changes are introduced. Finally, the supramolecular dynamics on different timescales are introduced briefly. In short, this chapter focuses on the fundamental spectroscopic principle, the most commonly used instruments, the experimental design and conduction, and the qualitative and quantitative analysis. Moreover, state of art and perspectives of studies using these spectroscopies are presented.

41.2 Absorbance and Fluorescence Spectroscopies in Supramolecular Chemistry

The absorbance and fluorescence spectroscopies are two commonly used methodologies to study the supramolecular chemistry including the molecular recognition, the self-process, and constitutional dynamic chemistry. These methodologies require that the system contains chromophores (to absorb light) or fluorophores to (emit light). Moreover, the signals of these materials should be changed during the supramolecular process. For those supramolecular systems that contain no chromophores or fluorophores, it is necessary to introduce into the systems the probes that

are sensitive and responsive to the change of their microenvironments triggered by the supramolecular processes. During the last decade, with the development of new technologies, transient spectroscopies were developed to probe and characterize the transient state (short-lived excited state) of the probe molecules on different time scales from nanosecond to microsecond and successfully employed to study the supramolecular processes.

In this section, several absorbance and fluorescence spectroscopies and their applications in the supramolecular study will be introduced.

41.2.1 General Preparation for Spectroscopies

41.2.1.1 The Selection of Probes

The probes need to be sensitive to the change of its microenvironment and selective to the specific binding sites. The probes could be an inherent part of the supramolecular systems. For example, a fluorescent-cavity pillararene was designed and synthesized by conjugating a chromophore to the host cavity, as shown in Fig. 1 [8]. This host can selectively detect succinonitrile with fluorescence enhancement at lower concentration of probes (5 μM) and malononitrile with fluorescence quenching at higher concentration of probes (0.1 mM). Such dramatically different signal responses on the guests with a subtle difference of one methylene group were attributed to the subtle difference of guest locations within the cavity.

On other hands, the probes need to be introduced into the supramolecular systems if the original systems are optically silent. The probes are diffused and then located in some specific locations mainly driven by the supramolecular interactions between the probes and the binding sites of the supramolecular systems. In general, one might be tempted to assume that the binding sites where the probes are located are identical and homogeneous. However, there might be many different binding sites with different sizes and binding affinities for the probes. For example, as shown in Fig. 2, there are at least five binding sites with different sizes and different hydrophobicities in human serum albumin (the host). As a result, the mobility and the dimerization reactivity of 2-anthracenecarboxylate (the guest) are different when located in different binding sites [9].

Another concern regarding the selection is the stability of the probes. The probes might become reactive when excited or suffer from photobleaching, adsorption, and precipitation. As a result, the probe signals detected for a supramolecular system might be artifacts or unrelated to the supramolecular processes, and thus interfere with the interpretation of the results. For example, during the study of the binding dynamics of 2-naphthyl-1-ethylammonium cation with cucurbit[7]uril, a product that emits at 450 nm was detected under the continuous irradiation of the aerated samples at high photon flux (Fig. 3) [10]. This probe was related to the presence of oxygen, the concentration of the host-guest complex, and the photon flux. However, it was not useful for probing the host-guest binding in the project and thus need to be suppressed.

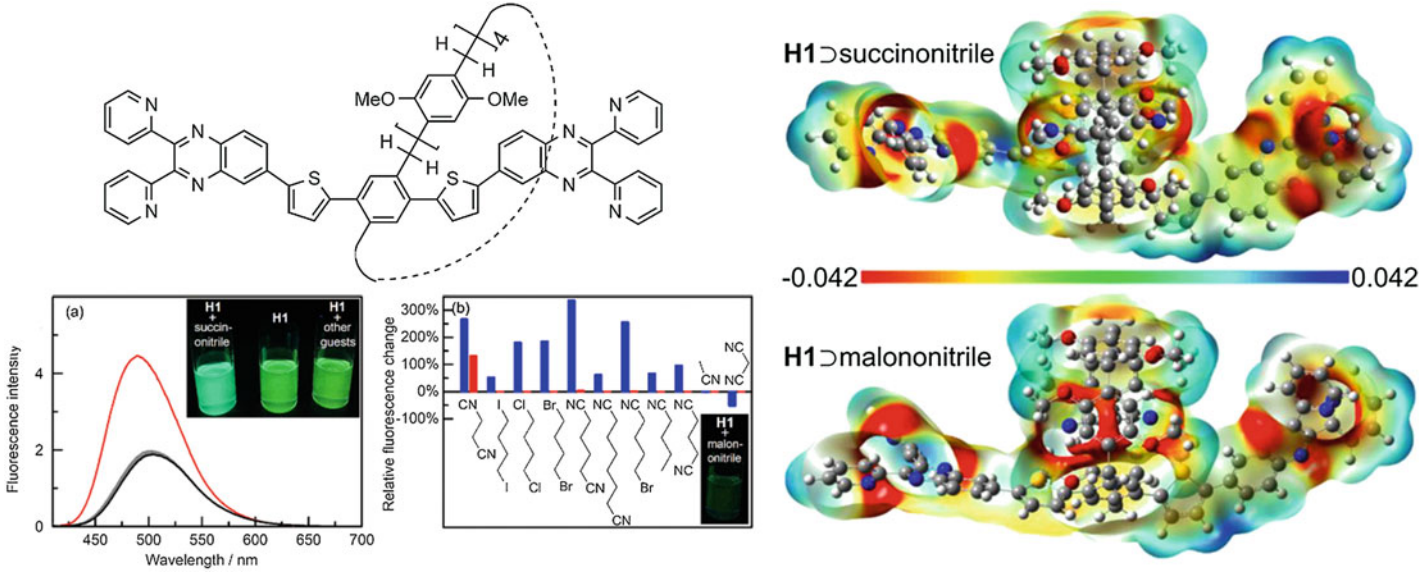

Fig. 1 Molecular structure of a fluorescent-cavity pillararene, its fluorescence response to different guests, and electrostatic potentials mapped on the electron isodensity surface of H1 ⊃ guests Ref. [8]

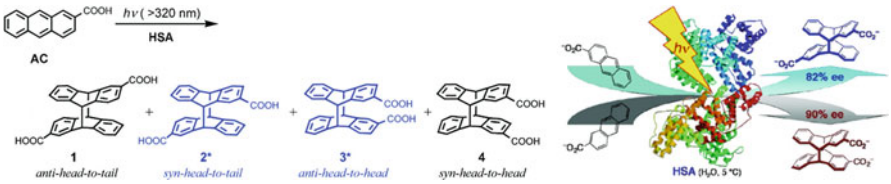

Fig. 2 Enantiodifferentiating photocyclodimerization of 2-anthracenecarboxylate (AC) mediated by different binding sites of human serum albumin (HAS) in aqueous solution Ref. [9]

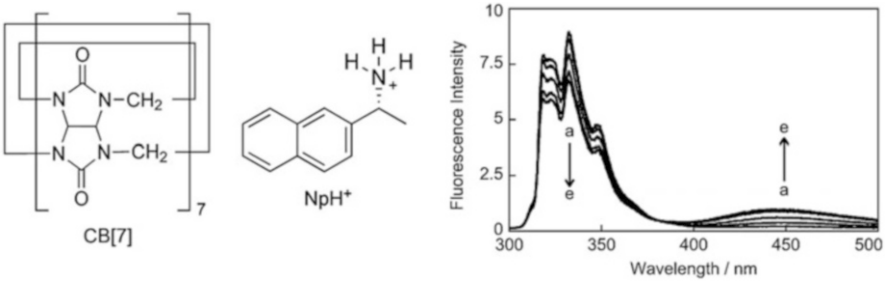

Fig. 3 Artifact observed at 450 nm over time during the binding of cucurbit[7]uril to 2-naphthyl-1-ethylammonium cation (NpH^+) in the presence of Na^+ in the aerated samples at high photon flux Ref. [10]

41.2.1.2 The Selection of Media

Important principles on the selection of solvents need to be considered including: (i) the solubility of the supramolecular components such as host molecules and guest molecules, (ii) the inertia to react with the supramolecular components, (iii) the inability to absorb or emit light at certain wavelengths that interfere with the spectra of the supramolecular systems, and (iv) the extra driving force from the interactions between the solvent molecules and the supramolecular components. For example, the per-methoxylated pillar[5]arene-guest complex were destabilized in polar solvents due to the strong interaction between the polar guests (dicyanoethane, 1,4-dibromobutane and 1,3-dicyanopropane) and the polar solvent. Moreover, when the solvent molecule was changed from p-xylene (that can bind into the host cavity) to *o*-xylene (that cannot bind into the cavity due to the steric hindrance effect), the binding affinity between the per-methoxylated pillar[5]arene and guests increased at least ten fold, showing a competition between the solvent molecule *p*-xylene and the guest for the binding site of the host. As a result, the binding affinity between per-methoxylated pillar[5]arene and dicyanoethane can change from 42 M^{-1} in acetonitrile to 1.8×10^6 M^{-1} in *o*-xylene, as shown in Fig. 4 [11]. Indeed, the host-guest complexation could even lead to the precipitation that can be easily observed by naked eyes [12].

In some cases, cosolvent or coion was added into the supramolecular system to solubilize the supramolecular components. For example, in the cucurbituril chemistry, the addition of metal ions or hydronium was necessary to solubilize the host

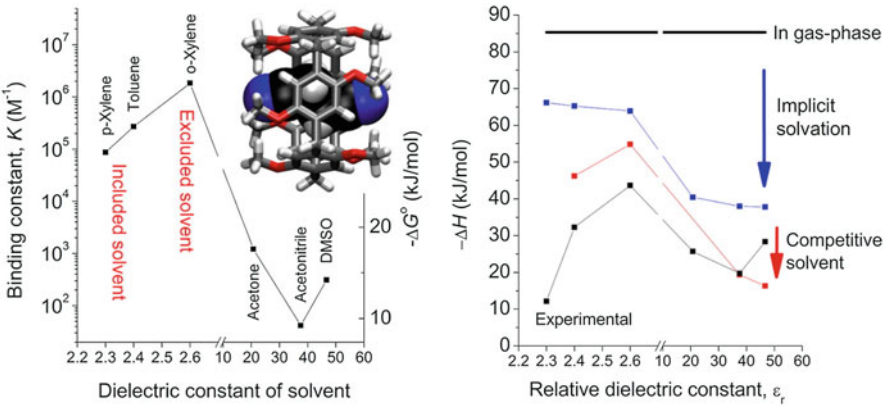

Fig. 4 Solvent effect on the binding affinity of per-methoxylated pillararene to dicyanoethane, and the goodness of fit of data when considering the dual roles of solvent molecules as the media and the competitor of the guest Ref. [11]

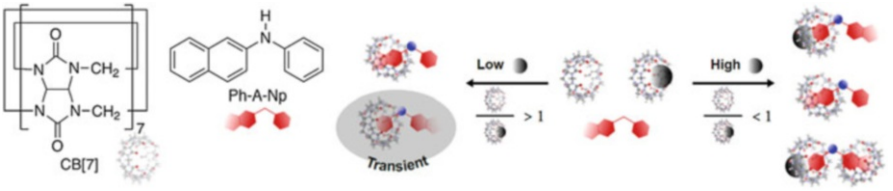

Fig. 5 The effect of Na^+ concentration on the distribution of species and the binding mechanisms for the Ph-H^+-Np/CB[7] system Ref. [17]

molecules in aqueous solutions. The presence of cocations (or hydronium) in general leads to the decrease of the binding affinity of host to guest because of the competition between the cocations and the guest to the binding sites of the host [10, 13–16]. Interesting, the presence of cocations with different concentrations can induce the formation of different types of host-guest complexes. For example, as shown in Fig. 5, at lower concentration of Na^+ ($\leq$5 mM), the naphthyl unit of N-phenyl-2-naphthylammonium cation (Ph-AH^+-Np) bind to the cavity of cucurbit[7]uril. In contrast, at higher concentration of Na^+ ($\geq$25 mM), the binding of Na^+ to CB[7] stabilized the binding of phenyl unit of Ph-AH^+-Np, and thus lead to the formation of Na^+•CB[7]@Ph-AH^+-Np@CB[7] 2:1 host–guest complex (where "@" and "•" represent an inclusion complex and an exclusion complex, respectively) [17].

41.2.1.3 The Selection of Laboratory Tools

Cuvettes are used to hold samples for the spectroscopic test. Theoretically they can be made by any materials that do not absorb the light at certain wavelengths. There are mainly three types of cuvettes including quartz, glass and plastic ones. Quartz cuvette can be used for the test from 190 nm – 2500 nm, but are quite expensive.

Glass one can be used in the range of 340 nm – 2500 nm and less expensive. Plastic cuvettes are transparent in the visible light range (380 nm – 780 nm), cheap and disposable with the cross-contamination of samples being avoided. However, they are unsuitable for the UV light range and can be corroded by many organic solvents. When choosing the right cuvette for the experiment, the researchers need to check the wavelength ranges, the solvents, and the photophysical properties of the samples. Another issue is related to the adsorption of the probe to glass and plastic surfaces that continuously decrease the concentration of probe in the solution and therefore decrease the absorbance or fluorescence signal. For example, the fluorescence of 1 μM Rhodamine 6G (the probe) decreased at least 15% and 40% within 5 h when hold in a quartz cuvette and in a borosilicate vial, respectively. The decrease was more dramatical when using a plastic vial. [18] The adsorption issue of probe becomes worse with a lower concentration of the dye prepared: In the same study, more than 90% of 10 nM Rhodamine 6G were lost during the sample preparation with glass or plastic containers [18]. The adsorption of Rhodamine 6G to the surfaces of equipment was suppressed in the presence of cucurbit[7]uril due to the host-guest complexation between the cucurbit[7]uril and Rhodamine 6G. Nevertheless, one might keep in mind that the concentration of hydrophobic dyes in aqueous solution might be largely overestimated especially when preparing the samples at low concentrations (μM or lower) or handling the samples with plastic laboratory tools such as plastic pipettes or cuvettes.

41.2.2 The Qualitative Spectroscopic Study

The signal changes of the probes upon supramolecular interactions could be the intensity changes for certain bands, or the wavelength shifts, or both. Several mechanisms for the signal changes were listed as examples.

41.2.2.1 The Intensity Changes

One general mechanism related to the intensity enhancement for the fluorescence of the probe is that the host cavity provides a protection for the excited-state probe against quenching by the quencher (such as oxygen or ions) in the solvents. In other cases, the energy transfer process (ET) or the charge transfer process (CT) between donor and acceptor could occur if the donor and the acceptor are in close proximity during the host-guest binding, leading to the fluorescence quenching of the donor. For the acceptor, the fluorescence could be enhanced in case of ET or quenched in case of CT. Furthermore, the close proximity of the polar moiety of one supramolecular component with the fluorophore of another component can be realized during the supramolecular process and leads to a polarity-induced fluorescence quenching.

Another mechanism related to the intensity change is the Ham effect proposed by Ham in 1953 [19, 20]. During the determination of the absorption of benzene, Ham found that the absorption band at 260 nm was enhanced with the solvent changing from a hydrocarbon solvent to carbon tetrachloride. This absorption enhancement of forbidden transitions of the solute was attributed to the overlap between the wave

functions of the excited-state solutes and those of the ground-state solvents with a positive electron affinity or a moderate ionization potential or both. This Ham effect was observed later for many symmetry aromatic molecules including naphthalene and pyrene since their first electronic transition are symmetry forbidden and can be enhanced when located in polar environments. Indeed, the strength of the 0–0 band for pyrene is very sensitive to the solvent polarity. As a result, the intensity ratio of the 0–0 band and the third band in vibronic fine structure of the fluorescence spectra of pyrene was developed as a "pyrene scale" to characterize the polarity of solvents [21, 22]. The "pyrene scale" was later employed to study the polarity of the host cavities for a synthetic cavitand octa acid [23, 24], β-cyclodextrin and so on [25].

The intensity change could be related to the aggregation process. In general, the fluorescence is often quenched for fluorophore at high concentrations due to the formation of aggregates, which is referred to as "aggregation-caused quenching" (ACQ). In contrast, a newly developed mechanism for the fluorescence enhancement is related to the aggregation induced emission (AIE), where the related materials are more emissive in the aggregated state [26–32]. Whether AIE or ACQ prevails in the systems depends on the molecular structure. For example, planar fluorophores tent to aggregate with the strong π-π stacking interactions between them, which leads to the fluorescence quenching, whereas the nonplanar fluorophores might have AIE properties due to the restriction of intramolecular rotation, the restriction of intramolecular vibrations, or both (i.e., the restriction of intramolecular motions). In the supramolecular system, the fluorescence enhancement might be observed during the binding of host to a guest with ACQ property, or during the crosslinking of polymeric host with AIE property by the binding of multitopic guest, or both [33, 34]. Recently, the concept of the assembling-induced emission was reported where the molecular motions and the emission are both controlled by the supramolecular dynamic assembling [35, 36].

41.2.2.2 The Wavelength Shifts

The general mechanism related to the wavelength shifts for the probes is the Franck-Condon principle in solvation. As shown in Fig. 6, the probes could interact with the solvent molecules via weak interactions with the energy of the interaction being

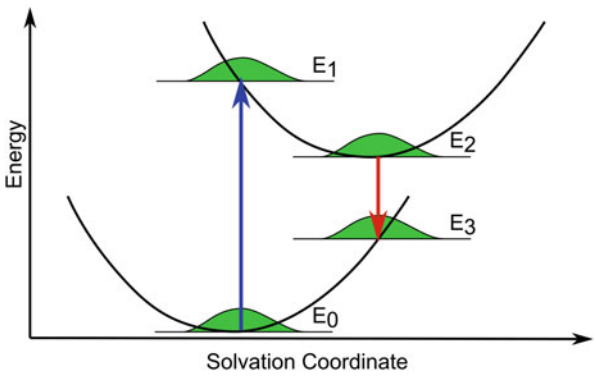

Fig. 6 Energy diagram for the Franck-Condon principle in solvation

minimized (energy level E_0). Upon the excitation of the probes, the electronic transition occurs at 10^{-15} second timescale, during which the positions of the probes and the solvent molecules stay the same (energy level E_1). The dipole moment of the excited state of probes may be different from that of the ground state of probes. As a result, the solvent molecules will rearrange around the probes to minimize the interaction energy (energy level E_2). If the lifetime of the excited state of the probe is longer than the time for the rearrange of the solvent molecules, the excited state of the probe would decay from E_2 to the ground state (energy level E_3), during which the positions of the probes and the solvent molecules stay the same. The interaction energy will be minimized by the rearrangement of the solvent molecules such that the system reaches E_0. If the excited state of the probe has a dipole moment larger than the ground state, the energy level E_2 and E_0 will be significantly lower than E_1 and E_3 in the presence of polar solvents, respectively. On the other hand, the absorption band of the probe is related to the transition from E_0 to E_1, while the fluorescence band is related to the transition from E_2 to E_3. Therefore, the fluorescence band for the probe with excited state more polar than its ground state will be red shifted in the presence of polar solvents. Moreover, the stoke shift will increase with the polarity of the solvents. In the case that the ground state of probes has a dipole moment larger than the excited state, a blue shift of the fluorescence band could be observed in the presence of polar solvents. Upon complexation, the probes move into the host cavities which are in general more hydrophobic than the solvent phase and have polarities different from the solvent phases, which could lead to a shift observed for the spectra.

41.2.3 The Quantitative Spectroscopic Study

41.2.3.1 The Relationship between the Signals and the Probe Concentration

The value of absorbance determined for a probe by using a colorimeter is independent on the equipment and proportional to the concentration of the probe according to Beer's law, (Eq. 1). It is convenient to determine the concentration of sample by the absorbance spectroscopy. For example, Kaifer developed a methodology to determine the purity of cucurbit[7]uril and cucurbit[8]uril [37]. The absorbance of the organometallic cobaltocenium cation decreased linearly with the addition of cucurbituril sample and reached a plateau when one equivalent of cucurbituril was added. The plot of absorbance against the concentration of cucurbituril was straightforwardly characterized by two straight lines with the intersection of two lines at the equivalence point.

$$A = \varepsilon \times L \times c \tag{1}$$

where A, ε, L, and c represent the absorbance of the probe, the molar extinction coefficient, the light path length of the sample, and the concentration of the probe, respectively.

In general, the fluorescence spectroscopy is more sensitive than the absorption spectroscopy. The value of fluorescence intensity, in contrast to that of absorbance, depends not only on the photophysical property (i.e., the fluorescence quantum yield) and the concentration of the probe but also on the setting of the fluorimeter such as the photon flux of lamp, the slit widths, the voltage applied to the photomultiplier, etc. Therefore, the values of fluorescence intensity for samples can be compared only when the experimental conditions are the same. The reason is discussed below.

$$I_F = I_0 \times \left(1 - 10^{-A}\right) \times \Phi_F \tag{2}$$

where I_F, I_0, and Φ_F represent the fluorescence intensity, the intensity of the incident light at the excitation wavelength, the fluorescence quantum yield of the probe, respectively.

Mathematical approximation (Eq. 3) is valid when the absorbance of the probe at the excitation wavelength is less than 0.2.

$$1 - 10^{-A} \approx R \times A \tag{3}$$

where $R = 2.205$ when $A < 0.2$.

The linear relationship between the fluorescence intensity (I_F) and the concentration of probe (C) is achieved (Eq. 4) by combining the Eqs. 1, 2, and 3.

$$I_F = I_0 \times R \times \varepsilon \times L \times \Phi_F \times c \tag{4}$$

It is worth noting that Eq. 4 is valid only under the condition that the absorbance of the probe at the excitation wavelength is less than 0.2. Higher absorbance values lead to deviation from the linear dependence of the fluorescence intensity on the concentration of the probe. Several methods can be used to lower the absorbance values at the excitation wavelength, including (i) shifting the excitation wavelength to a region where the absorbance is lower, (ii) diluting the solution, and (iii) using a cuvette with shorter light path (e.g., 1 mm or 2 mm) than the standard cuvette (10 mm).

41.2.3.2 The Determination of Lifetime of the Singlet Excited State

The fluorescence quantum yield Φ_F in Eq. 2 is related to the rate constant for the fluorescence from the singlet-excited species (k_F) and the lifetime for the singlet-excited species (τ), as shown in Eq. 5. The rate constant k_F is related to the refractive index of the medium, the oscillator strength, and the wavenumber corresponding to the maximum wavelength of absorption [38]. In general, the oscillator strength of fluorescence dyes are insensitive to the environment where the dyes are located [39]. The lifetime τ is the reciprocal of the sum of rates for all possible deexcitation pathways and can be determined by using the single photon counting technique.

$$\Phi_F = k_F \times \tau \tag{5}$$

For a supramolecular system where multiple fluorescent species (i) coexist, the fluorescence decays are fit to a sum of exponentials (Eq. 6) with the lifetimes (τ_i) and the pre-exponential factors (A_i) being determined. The quality of each fit was judged by the residuals plot and the value of χ^2. The number of exponentials (n) for each fit was increased until the residuals were random and the χ^2 values were between 0.9 and 1.2. It is worth noting that evaluating the goodness of the fit solely by the value of χ^2 is sometimes misleading since the value of χ^2 can be within the range of 0.9–1.2 even when the goodness of fit is poor with the residuals being non-random. Therefore, always check the residuals plot during the data treatment.

$$I_{\mathrm{t}} = I_0 \times \sum_{i=1}^{n} \left[A_{\mathrm{i}} \times e^{-\frac{t}{\tau_{\mathrm{i}}}} \right] \tag{6}$$

The fluorescence intensities for each species (e.g., a system with two species i and j) can be related to the pre-exponential factor and singlet-excited state lifetime τ by Eq. 7. Equation 8 is then derived from Eq. 7.

$$\frac{I_{\mathrm{F,i}}}{I_{\mathrm{F,j}}} = \frac{\int_0^{\infty} \left(A_{\mathrm{i}} \times e^{-\frac{t}{\tau_{\mathrm{i}}}} \right)}{\int_0^{\infty} \left(A_{\mathrm{j}} \times e^{-\frac{t}{\tau_{\mathrm{j}}}} \right)} \tag{7}$$

$$\frac{I_{\mathrm{F,i}}}{I_{\mathrm{F,j}}} = \frac{A_{\mathrm{i}} \tau_{\mathrm{i}}}{A_{\mathrm{j}} \tau_{\mathrm{j}}} \tag{8}$$

According to Eq. 4, the fluorescence intensities for each species can be related to the concentration of each species by Eq. 9.

$$\frac{I_{\mathrm{F,i}}}{I_{\mathrm{F,j}}} = \frac{\varepsilon_{\mathrm{i}} \times k_{\mathrm{F,i}} \times \tau_{\mathrm{i}} \times [i]}{\varepsilon_{\mathrm{j}} \times k_{\mathrm{F,j}} \times \tau_{\mathrm{j}} \times [j]} \tag{9}$$

Eq 10 can be derived by associating Eqs. 8 and 9.

$$\frac{A_{\mathrm{i}}}{A_{\mathrm{j}}} = \quad g_{\mathrm{i,j}} \times \frac{[i]}{[j]} \tag{10}$$

where

$$g_{\mathrm{i,j}} = \frac{\varepsilon_{\mathrm{i}} \times k_{\mathrm{F,i}}}{\varepsilon_{\mathrm{j}} \times k_{\mathrm{F,j}}} \tag{11}$$

As a result, the ratio of pre-exponential factors for different species could be used to probe the ratio of concentrations for those species. For example, each enantiomer of 2-naphthyl-1-ethanol (*R*-NpOH or *S*-NpOH) binds to β-cyclodextrin to form two type of 1:1 complexes (N and E) [40]. N and E referred to the complexes with the naphthyl unit and with the ethanol unit of NpOH being deeply embeded into the β-cyclodextrin cavity, respectively. N and E could associate with each other to form

Table 1 Lifetimes and pre-exponential factors for the emission of NpOH obtained from the global analysis for the decay excited at 277 nm and measured at 380 nm [40]

NpOH	τ_1/ns	A_1	τ_2/ns	A_2	τ_3/ns	A_3
R-	25.4	0.17	38.0	0.11	72.7	0.72
S-	25.4	0.21	38.0	0.38	72.0	0.42

three type of 2:2 complexes, i.e., NN, EE, and NE, where the EE complexe exhibited excimer emission. The time-correlated single-photon counting experiments were conducted for the β-cyclodextrin/NpOH systems. The decays traces determined were fit by Eq. 6 with the parameter n being increased. The residuals between the data and the fit was not random until n was assigned to 3, implying a "best fit" with three fluorecent species being identified. The shortest lifetime, τ_1, was assigned to NpOH free in water, while the second lifetime, τ_2, was assigned to NpOH in the 1:1 host/guest complex. The longest lifetime, τ_3, corresponds to the excimer emission of NpOH in the 2:2 host/guest complex. The A_3 value is significantly higher for *R*-NpOH than for *S*-NpOH, indicating that more 2:2 host/guest complexes were formed for *R*-NpOH than for *S*-NpOH, and thus a chiral recognition (Table 1).

41.2.3.3 The Determination of Equilibrium Binding Constant

The absorbance or fluorescence intensity change at certain wavelength upon the host-guest complexation can be used to quantitatively study the host-guest binding. The host-guest binding ratio can be determined by a Job plot [41]. In the experiments, the samples are prepared with the concentration of guest varied but the total concentration of host and guest remaining constant. The signal change of absorbance or fluorescence intensity is then plotted against the mole fraction. The mole fraction with the maximum of the signal change in the plot implicates the host-guest binding ratio. The Job plot is simple and straightforward methodology to determine the binding ratio. However, one could determine the binding ratio and the equilibrium binding constant for the host-guest binding simultaneously by a titration experiment.

In the titration experiment, the concentration of the probe (either host or guest depending on which one is detectable) is in general kept constant while the concentration of the other species is varied. The signal changes are then plotted against the concentration of the titrant and the binding isotherm was fit with several binding models until the best fit was achieved. The goodness of the fit of a binding model is judged by the randomness of the distribution of residuals between the data and the fit. For example, the binding isotherms for the interaction of pillararene unit with multitopic guests were determined and fit with different binding model (Fig. 7) [33]. Only the fit with 2:1 host/guest binding model showed random residuals for the pillararene/ditopic guest complex and the fit with 3:1 host/guest binding model showed random residuals for the pillararene/tritopic guest complex, respectively.

It is worth noting that some traditional fitting methods, e.g., the Benesi-Hildebrand treatment for a 1:1 host-guest complex (Eq. 12) [42], are still employed nowadays. These methods are convenient and straightforward to fit the data using linear regression. However, these methods give higher weight to the lower signal

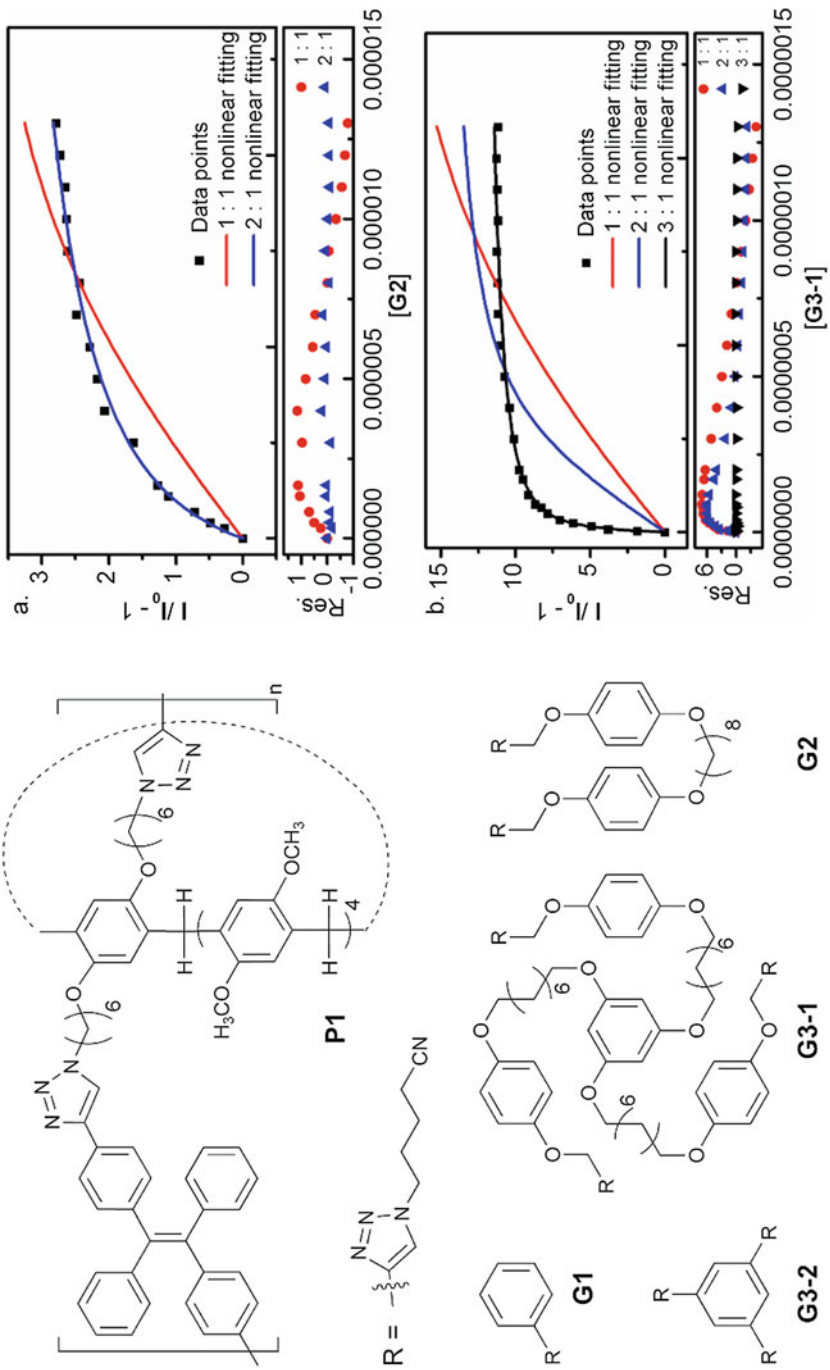

Fig. 7 The fit of binding isotherm with different host-guest binding models by the nonlinear regression Ref. [33]

changes which are determined at lower concentration of titrant and thus have the higher uncertainty. As a result, the equilibrium binding constant recovered by the linear regression (e.g., Eq. 12 for a 1:1 host-guest complex) is not so accurate as that determined by the nonlinear regression (e.g., Eq. 13 for a 1:1 host-guest complex).

$$\frac{1}{\Delta} = \frac{1}{\Delta'} + \frac{1}{K \times \Delta' \times \mathrm{c}} \tag{12}$$

$$\Delta = \frac{\Delta' \times K \times c}{1 + K \times c} \tag{13}$$

where Δ, Δ', K, and c represent the signal changes determined for each sample, the signal change between the free and complexed probe, the equilibrium binding constant, and the concentration of titrant, respectively.

41.3 NMR Spectroscopies in Supramolecular Chemistry

NMR spectroscopy is the very important and powerful methodology for the investigation of supramolecular systems. Various NMR techniques are applied to develop detailed structural elucidation of supramolecular systems and to study their thermodynamic and dynamic properties [5]. In this section, some most common NMR techniques and their applications in supramolecular systems will be given brief introduction.

Before beginning, it needs to be aware of that the host-guest complexation is a dynamic process. If there is a slow exchange between the free and bound species, separated NMR resonances will be observed for all species involved in the host-guest bonding equilibrium. However, the most common situation in host-guest complexation is a fast exchange, and the observed chemical shifts in this case is a weighted average of the values in the free and bound states [6].

41.3.1 1D NMR Spectroscopy

Changes in the 1D spectra of the molecules during a molecular assembly process can present the information about the resulting structure. Chemical shift change is usually an indicator of the formation of a host-guest complex, and more if it is informative on the binding mode analysis [5]. A recent and typical example has been provide by Yu liu and co-workers [43], where a variety of morphologically interesting aggregates have been constructed using bipyridinium-modified diphenylalanine derivative (BP-FF) and macrocyclic hosts (cucurbit[7]uril (CB[7]), cucurbit[8]uril (CB[8]), pillar[5]arene (WP5A), or tetrasulfonated crown ether (DNC)). There is the 1:1 complex stoichiometry between BP-FF and four macrocycles. Their binding modes were investigated by ^{1}H NMR spectroscopy. The NMR spectra of free host or guest molecules without binding were shown in Fig. 8a, c, e, g, i, respectively. The

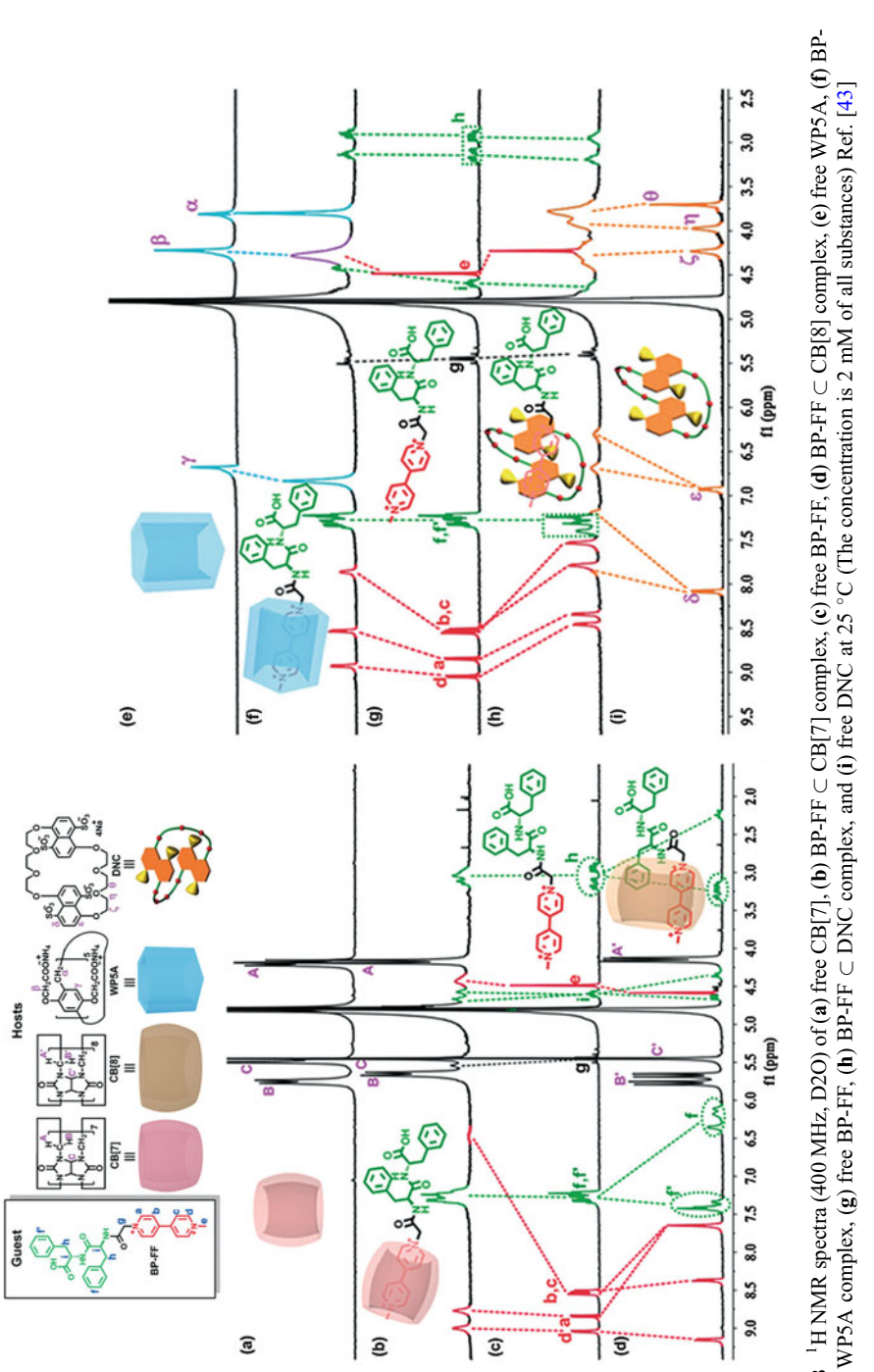

Fig. 8 ^{1}H NMR spectra (400 MHz, D2O) of (**a**) free CB[7], (**b**) BP-FF ⊂ CB[7] complex, (**c**) free BP-FF, (**d**) BP-FF ⊂ CB[8] complex, (**e**) free WP5A, (**f**) BP-FF ⊂ WP5A complex, (**g**) free BP-FF, (**h**) BP-FF ⊂ DNC complex, and (**i**) free DNC at 25 °C (The concentration is 2 mM of all substances) Ref. [43]

resonances of an included guest are usually shifted to upfield compared with the free molecule, due to the anisotropic effect of a rich electronic cavity of the host, such as the host with the aromatic walls [44]. When BP-FF ⊂ CB[7] complex formed, the protons (H_b and H_c) of the pyridinium moiety in BP-FF exhibited a large upfield shift in the presence of CB[7], while the protons of the phenyl rings were essentially unchanged (Fig. 8b, c). Therefore, it can be deduced that pyridinium moiety was bound to CB[7], but the diphenylalanine moiety is outside the cavity. In BP-FF ⊂ CB[8] complex, both pyridinium (H_a, H_b and H_c in Fig. 8d) and partial phenyl protons shifted to higher field in the presence of CB[8], indicating that the pyridinium moiety and phenyl ring of diphenylalanine were concurrently included in the cavity of CB[8]. As shown in Fig. 8f, when WP5A was added, the proton peaks of the pyridinium ring of BP-FF underwent an upfield shift, which demonstrate the host-guest inclusion between WP5A and the pyridinium moiety of BP-FF in water. Similarly, as can be seen from Fig. 8h, the chemical shifts of aromatic protons in DNC and all protons in bipyridinium moiety of BP-FF showed an upfield shift upon complexation with each other, by the anisotropic effect between naphthalene and pyridinium rings.

Chemical shift changes in 1D NMR spectroscopy are also usually utilized to study stimulus-response behaviors, intra- and intermolecular [6]. For example, the changes can reveal the conformational variation of host/guest, or the relative motions between molecules in a supramolecular system, such as in a rotaxane or catenane. As shown in Fig. 9, $OPVEx^2Box^{4+}$ is a semi-rigid tetra-cationic cyclophane with a rectangle-like geometry [45]. It comprises oligo(p-phenylenevinylene) pyridinium units and the biphenylene-bridged 4,4-bipyridinium extended viologens, where the stilbene part is photo- and thermal-responsive. (*EE*)-$OPVEx^2Box^{4+}$ can undergo (E)↔(Z) isomerization of vinyl group upon light irradiation or on heating. The photoisomerization can be displayed by ^{1}H NMR spectroscopy. The ^{1}H NMR spectrum of a freshly prepared (*EE*)-$OPVEx^2Box^{4+}$ sample under blue light (450–460 nm) irradiation showed two distinct proton resonances shifts to upfield of hydrogen in the alkene group (H_k and H_l), indicative of (*EE*)-$OPVEx^2Box^{4+}$ undergoing isomerization. More specifically, the resonances of the protons H_k and H_l were split into two sets: the original set was assigned to the unreacted *E* conformation, while the other set of proton resonances (Fig. 9b), H_o (*d*, J = 12.9 Hz) and H_p (*d*, J = 12.8 Hz), was corresponding to the transformation of $OPVEx^2Box^{4+}$ from the (*EE*)- to the (*EZ*)-isomer. On heating of the solution of the (EZ)-$OPVEx^2Box^{4+}$ at 70 °C for 16 h, the ^{1}H NMR spectra (Fig. 9c) was restored to the same as the (*EE*)-$OPVEx^2Box^{4+}$, which indicated almost quantitative thermalisomerization from the (*EZ*)-isomer to the (*EE*)-isomer.

In supramolecular chemistry study, it is a matter of great concern to study the controlled motion between molecules, because it is an important foundation of molecular machine research [46]. As mentioned above, certain chemical shift changes in 1D NMR spectroscopy are signs to tracking the relative motions between molecules. Wei jiang and co-workers has reported a rotaxane-based molecular shuttle that can achieve directional shuttling of a cone-like “rotor” on a symmetric “axle” [47]. The “rotor” was a naphthotube macrocycle, and the “axle” possessed

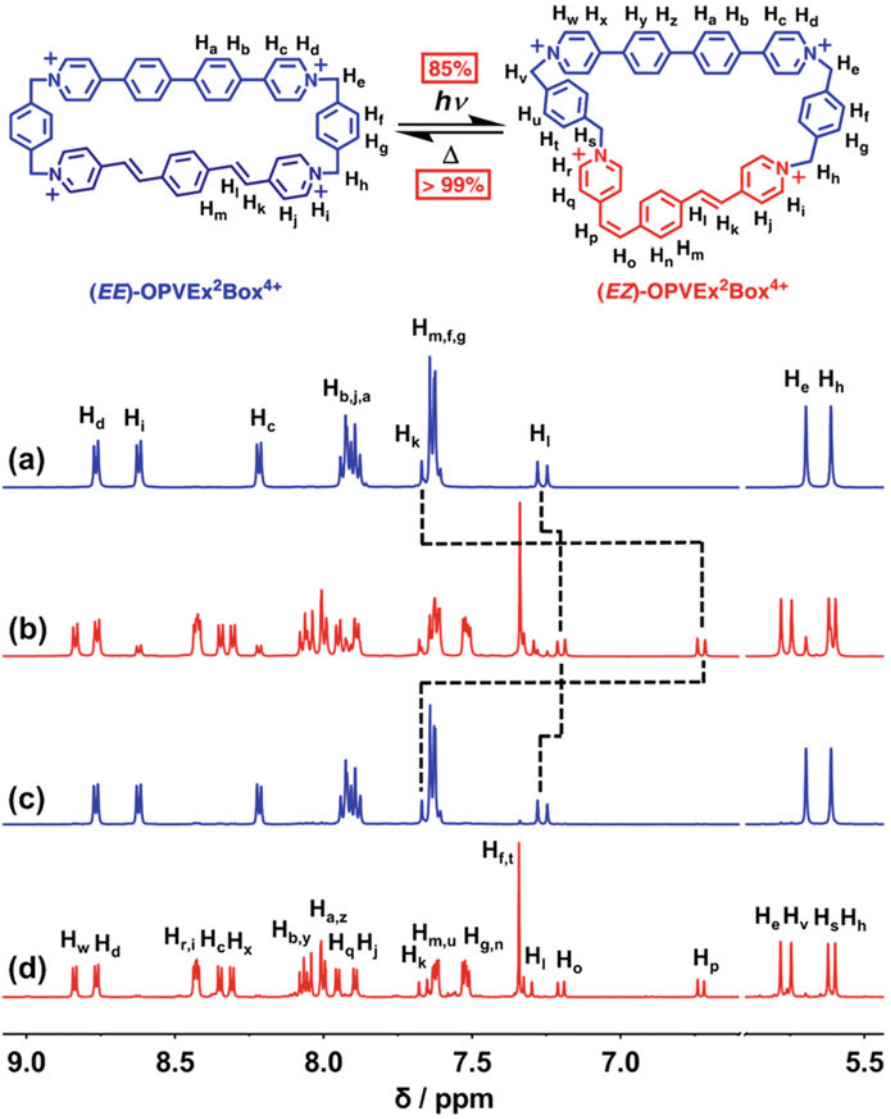

Fig. 9 ^{1}H NMR spectra (500 MHz, CD_3CN, 25 °C) of (EE)-OPVEx^{2}Box·4PF_6 (**a**) before and (**b**) after blue light irradiation (450–460 nm, 12 W, 12 s). (**c**) Spectrum after heating the solution of (**b**) for 16 h at 70 °C. (**d**) Spectrum of (EZ)-OPVEx^{2}Box·4PF_6 Ref. [45]

two phenyl triazole stations arranged in opposite orientations and one di(quaternary ammonium) station in the middle (Fig. 10a). The stimuli-responsive motion between the "rotor" and the "axle" in the rotaxane (R^{2+}) could be manipulated by the acid/base adding as shown in Fig. 10b. Its unique directional shuttling was discovered and supported from its ^{1}H NMR experiments. The addition of three equivalents TFA

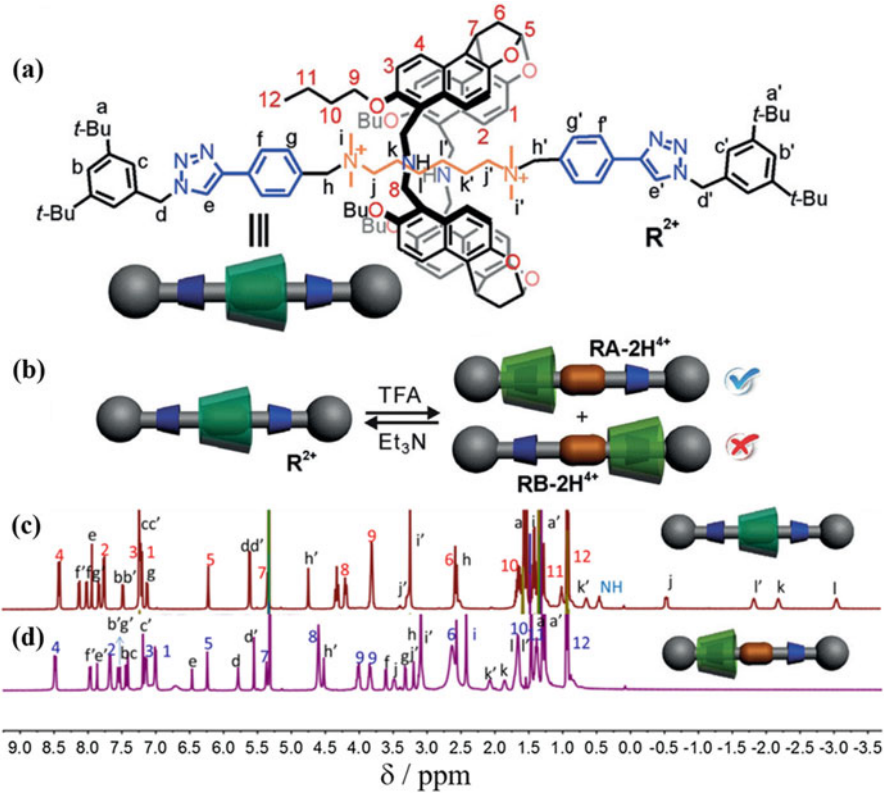

Fig. 10 (**a**) Chemical structure and cartoon of rotaxane R^{2+} with PF_6^- as the counterions. (**b**) Cartoon representation of acid/base controlled shuttling of rotaxane R^{2+}. ^{1}H NMR spectra (400 MHz, CD_2Cl_2, 2.0 mM, 25 °C) of rotaxane R^{2+} with PF_6^- in (**c**) the absence or (**d**) the presence of TFA Ref. [47]

into the solution of R^{2+} was able to cause the protonation of macrocycle and then the relocation of macrocycle to the two phenyl triazole stations. Because the upfield peaks of H atoms (H_j, H_k, H_l, $H_{k'}$, and $H_{l'}$) from the alkyl in the "axle" was disappeared, indicating the shielding effect faded away, that is, the electron-rich cavity of macrocycle moved away from the alkyl. It might result in the formation of two possible isomers RA-2H^{4+} and RB-2H^{4+}, if the movement of macrocycle was nondirectional onto the "axle." However, the ^{1}H NMR spectrum of R^{2+}in the presence of TFA was quite well-defined and clean, and only one set of isomer's signals was observed, standing for only one isomer exists. As regards peaks, protons in left phenyl triazole part underwent very large upfield shift, where H_e shifted upfield (−1.55 ppm), H_f (−4.72 ppm) and H_g (−3.47 ppm). These chemical shift changes revealed only RA-2H^{4+} was formed form the directional shuttling in the R^{2+}.

41.3.2 2D NMR Spectroscopy

2D NMR spectroscopy gives data plotted in a space defined by two frequency axes rather than one. The development from 1D to 2D NMR has opened a broader prospect for the application of nuclear magnetic technology. 2D NMR techniques have become very popular because they can easily and clearly show the interaction within or between molecules. The interactions through scalar couplings between nuclei can be detected mainly by COSY, TOCSY, HMQC, and HMBC experiments, while ones through space couplings is usually detected by NOESY and ROESY experiments.

2D COSY, called correlation spectroscopy, experiment is the simple and widely used 2D NMR experiment. It is an homonuclear chemical shift correlation experiment based on the transfer polarization by a mixing pulse between directly J-coupled spins, and homonuclear through-bond interactions can be trace out in its map if their cross-peak exists [48]. Thus, the spectral assignment in a complicated system can be made with the help of 2D COSY spectrum. In the work just mentioned about the directional shuttling of rotaxane R^{2+} [47], the identification of its ^1H NMR peaks to corresponding hydrogens of R^{2+}, especially the peaks of right (or left) "axle," is very difficult. To minimize form complexity, it is necessary to determine the peaks derived from the hydrogens on adjacent carbon (*e. g.*, $H_j - H_k$) through the cross-peaks in the 2D COSY map, as shown as in Fig. 11.

NOESY, called nuclear overhauser enhancement spectroscopy, is based on nuclear overhauser effects (NOE), and the NOE is defined as the change in the intensity of one spin when the spin transition of another nuclei nearby is perturbed from equilibrium population [48]. The NOE decreases rapidly with the increment of the distance between the nuclei, and thus the NOE cross peak in 2D map only relates protons which are spatially close to each other (closer than 0.4 nm), even if no chemical bonds connection, and the relative intensities of these cross-peaks depend on the spaces between the corresponding nuclei. When the molecules with a mass of 1000 Da – 2000 Da, it is worth noting the NOE can become very weak or even vanish. In that case, the spin-lock experiments such as the rotating frame NOE (ROESY) should be used instead of NOESY. Thus, NOESY and ROESY are very useful for judging protons that are close to each other in the supermolecular structure. For example, the structure of β-cyclodextrin/BPA complex was investigated in water solution by ROESY experiments at 25 °C in D_2O [49]. As shown in Fig. 12, β-cyclodextrin is a cyclic oligosaccharide with seven D-glucose units linked by α-1,4-glucose bonds and has the H_3/H_5 inside its hydrophobic cavity. H_3 locates at the secondary ring side, while H_5 at the primary ring side. β-cyclodextrin can form 1:1 complex with BPA, and the ROESY spectrum of the complex displayed clear NOE cross-peaks between the H_a proton of BPA and the H_3/H_5 protons of β-cyclodextrin (peaks A and B), as well as, between the H_b protons of BPA and the H_3/H_5 protons of β-cyclodextrin (peaks C and D). These NOE cross-peaks indicate the structure of the complex, where the phenyl ring of BPA is deeply included into the β-cyclodextrin's cavity. Moreover, considering the comparable intensity of peaks E and F (peaks E assigned to the NOE cross-peaks between the H_c and H_3, peaks F

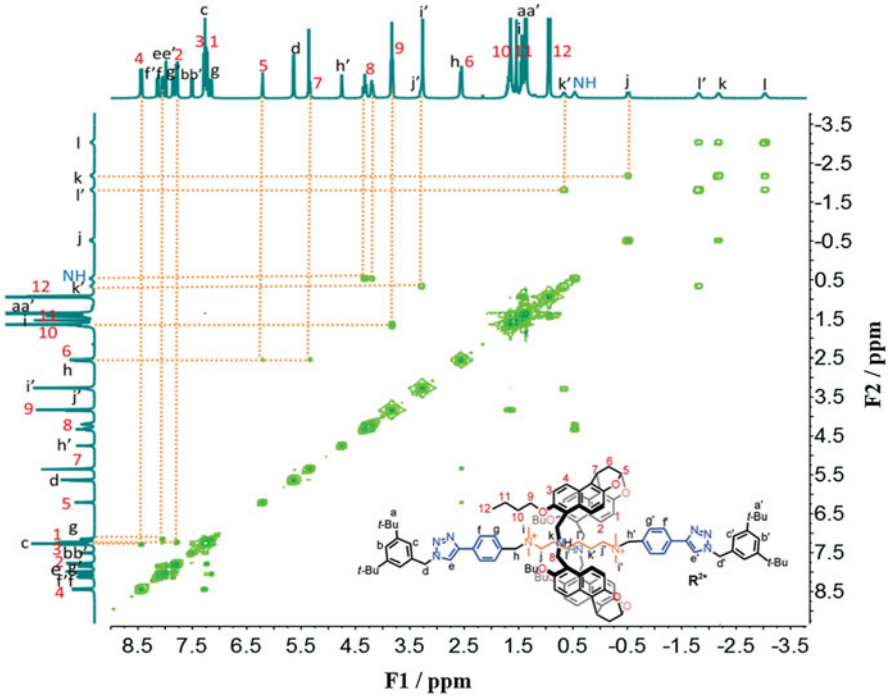

Fig. 11 2D ^{1}H-^{1}H COSY spectrum of (400 MHz, CD_2Cl_2, 2.0 mM, 25 °C) of rotaxane R^{2+} with PF_6^- Ref. [47]

assigned to the NOE cross-peaks between the H_c and H_5), the BPA molecule can puncture simultaneously into the β-cyclodextrin's cavity both from the primary ring side and the secondary ring side. From a NOESY spectrum, similar information can be obtained. As shown in Fig. 13, the pillararene (WP5-P) and the guest (G1) displayed NOE cross peaks between protons H_a, H_b, and H_c of WP5-P and protons H_1 and H_4 of G1 in their NOESY spectrum, indicating the complex can be formed and has the structure as presented in Fig. 13a [50].

41.3.3 DOSY Technique

The diffusion coefficients (D) can be calculated by the Stokes-Einstein equation (Eq. 14):

$$D = \frac{k_B T}{6\pi\eta r} \tag{14}$$

where k_B is the Boltzmann constant, T is the absolute temperature, η is the dynamic viscosity, and r is the hydrodynamic radius of the species [51]. The diffusion

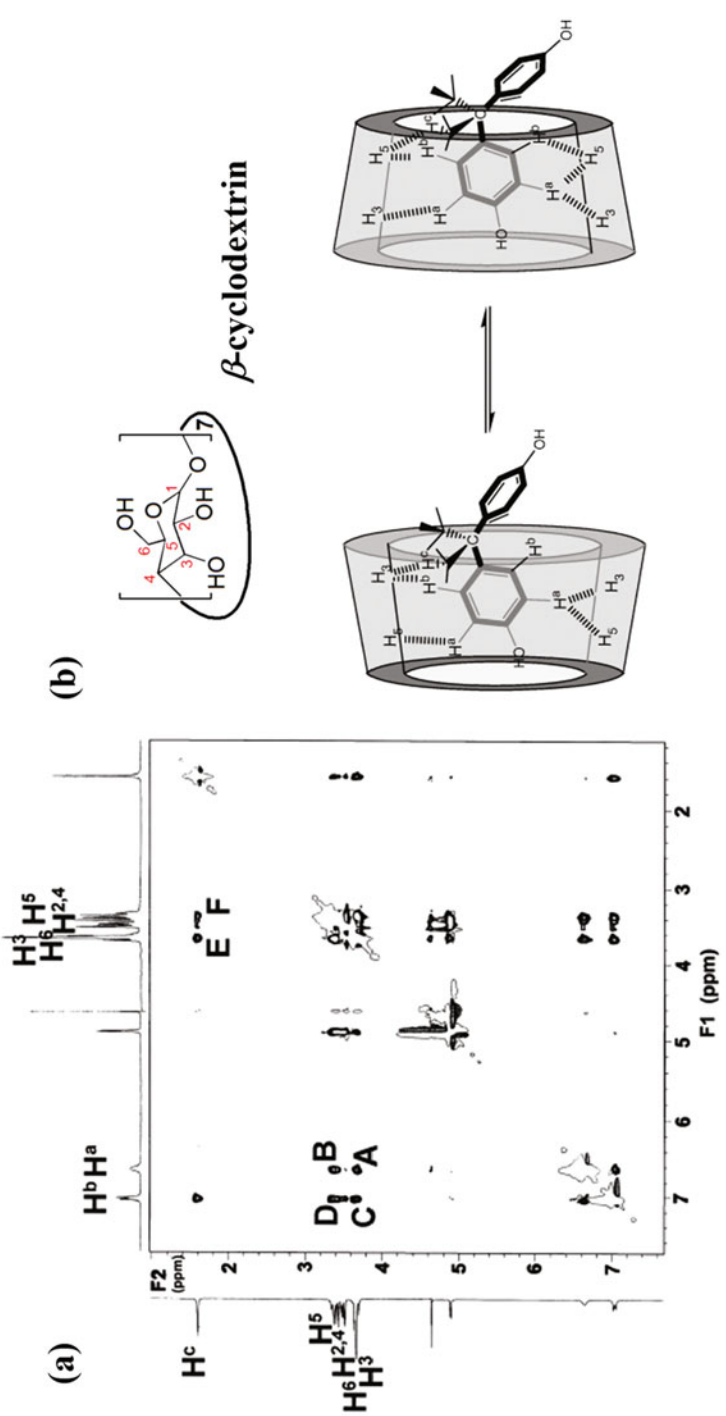

Fig. 12 (**a**) ^{1}H ROESY spectrum of the β-cyclodextrin/BPA complex (8 mM in D_2O at 25 °C with a mixing time of 200 ms). (**b**) Possible structure of the complex in aqueous solution [49]

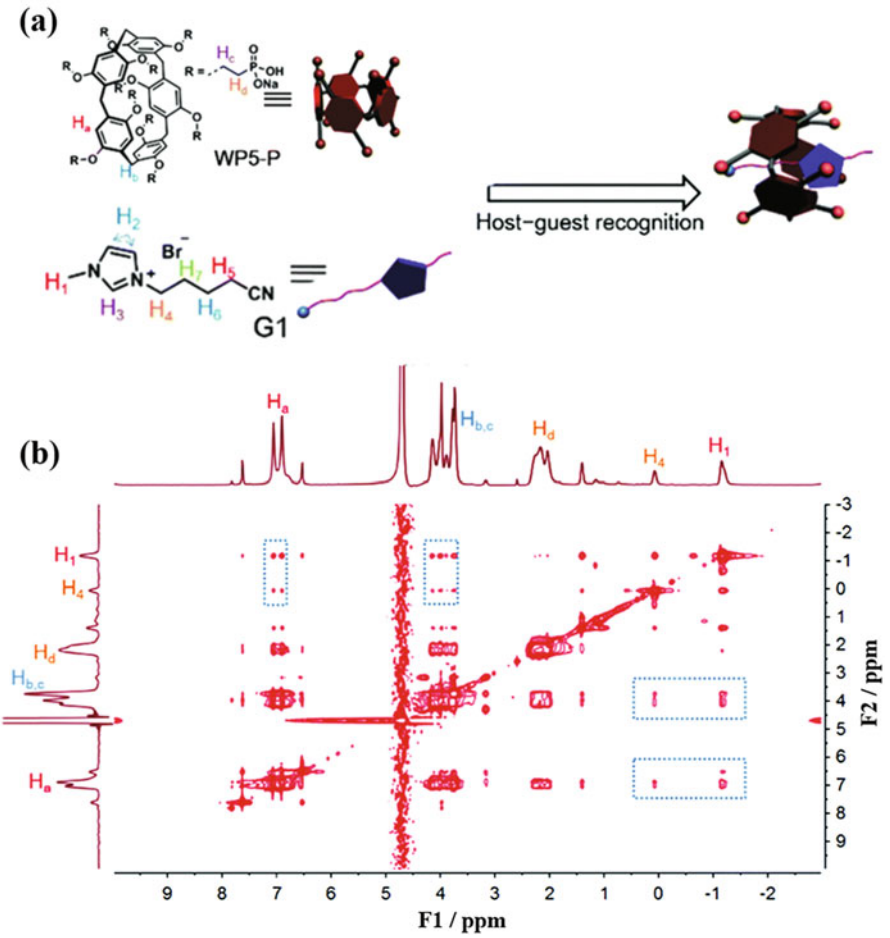

Fig. 13 (**a**) Structures and cartoon representations of WP5-P/G1, (**b**) ^{1}H NOESY spectrum of a mixture of WP5-P (10.0 mM) and G1(10.0 mM). The NOE correlation signals that confirm the host-guest interactions are marked on the spectrum Ref. [50]

coefficients, in a given situation can reflect on the size and shape of species. Since molecular aggregations and complexations in solution will cause a change in the diffusion coefficients, diffusion measurements are attracting more attention in supramolecular chemistry. Many NMR techniques are developed for diffusion measurements to investigate molecular interactions, such as DOSY. DOSY, called diffusion-ordered NMR spectroscopy, is also presented as a 2D map with the chemical shift in the horizontal axis and the diffusion coefficient of the component in the vertical axis [52], so it shows the separation of the components in a complex mixture according to their diffusion coefficient just like a "NMR chromatography" and make an evaluation of the species in equilibrium. Cohen and co-workers confirmed the hexameric capsules of M1 formed in $CDCl_3$ by the DOSY experiment using M2 as an internal

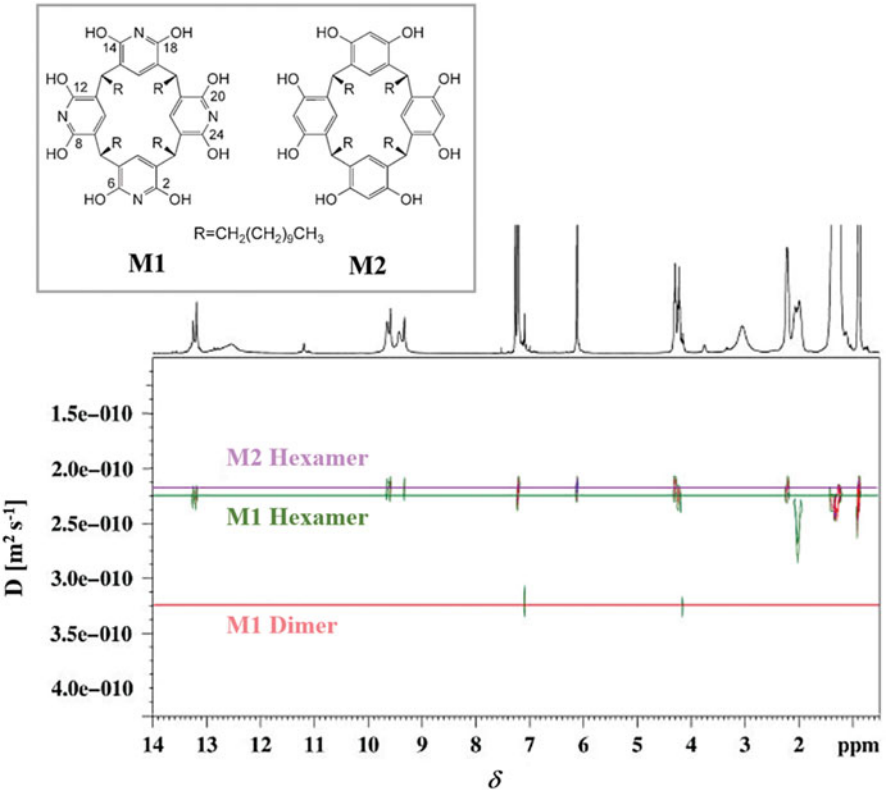

Fig. 14 ^{1}H DOSY of a mixture of M1 (20mM) and M2 (20mM) in $CDCl_3$ at 25 °C. Structures of M1 and M2 as shown on top Ref. [53]

reference [53]. The DOSY spectrum of the 1:1 mixture of M1/M2 (Fig. 14) shows three diffusing sets of peaks. M2 is known to form robust hexamers when dissolved in $CDCl_3$, so the horizontal purple line represents the diffusion value of its hexamers. The diffusion coefficient of the slower diffusing set of peaks of M1 (green line) is approximate to that of the hexamer of M2, indicating the hexamers M1 formed. In addition, the red line indicates the diffusion value of the dimer of M1.

41.3.4 NMR Titration

NMR titration is measurement of chemical shift changes as a function of concentrations of species. As mentioned above, if host-guest complexation is a fast exchange, the observed chemical shift in this case is a weighted average of the values in the free and bound states. Thus, in that situation, the association constant (K) of host-guest complexation can then be obtained from a series of NMR spectra measured at different initial concentrations of host and guest. The data treatment

with Benesi-Hildebrand equation is recommended and like that of the spectral methods in previous section (Eq. 6). The advantage of NMR technology is that it can provide more microscopic information for complicated supramolecular structures and avoid mistakes attributed to the presence of impurities. For example, Yuliu and co-workers employed a ^{1}H NMR titration to investigate the association constants (K) of CPT-CD and ADA-EDA [54]. CPT-CD and ADA-EDA are derivatives of β-cyclodextrin and adamantane, respectively. Firstly, the stoichiometry between CPT-CD and ADA-EDA was determined as 1:1 according to the Job's plot where the maximum was observed at a molar fraction of 0.5. As shown in Fig. 15, the concentration of ADA-EDA was fixed at 0.5 mM, and the concentration of CPT-CD increased from 0 to 3.0 mM. The proton signals of ADA-EDA shifted downfield gradually for the inclusion of ADA part into the cavity of CPT-CD. The peak at $\delta = 1.86$ ppm is assigned to ADA-EDA, and its chemical-shift changes is chosen as the function of the concentration of CPT-CD by analyzing the nonlinear least-squares fit. Finally, the binding constant (K) between ADA-EDA and CPT-CD was calculated as $(1.8 \pm 0.2) \times 10^3\ M^{-1}$.

41.4 CD Spectroscopy in Supramolecular Chemistry

41.4.1 Generation of ICD

Circular dichroism (CD) is a chiroptical spectroscopy, and the phenomenon of CD is derived from the differential absorption, usually in the UV-Vis wavelength region, of molecules with left- and right-circularly polarized light (CPL) [55]. Its signal can be positive or negative, depending on whether left-CPL is absorbed to a greater extent than right-CPL. A chiral molecule is optically active, so CD spectroscopy is a sensitive spectroscopic tool for determining its absolute configurations and conformations. Nevertheless, an achiral molecule can be induced optical activity by a chiral and transparent molecule as result of the appropriate coupling between the electrical transition moments of the former and of the latter, that is, it displays induced circular dichroism (ICD) signals in absorption bands after complexation with a chiral inducing molecule [7, 56]. The basic idea of ICD is shown in Fig. 16.

A good example for ICD caused by hosts is that achiral naphthalene derivatives can be endowed ICD property by the complexation with cyclodextrins [57]. Cyclodextrins are chiral molecules but do not absorb in the UV-Vis region and consequently do not show CD over there. Achiral naphthalene derivatives can absorb in this wavelength range, but CD inactive. When the naphthalene guest complexes with a cyclodextrin, it arises the ICD in the UV-Vis region [58–61].

41.4.2 Kodaka's Rules

Kodaka proposed some general rules for ICD of an achiral chromophore caused by a chiral macrocycle host, in particular for cyclodextrins [58–60]. (1) For the guest included in the host, an electronic transition of achiral guest parallel to the axis of

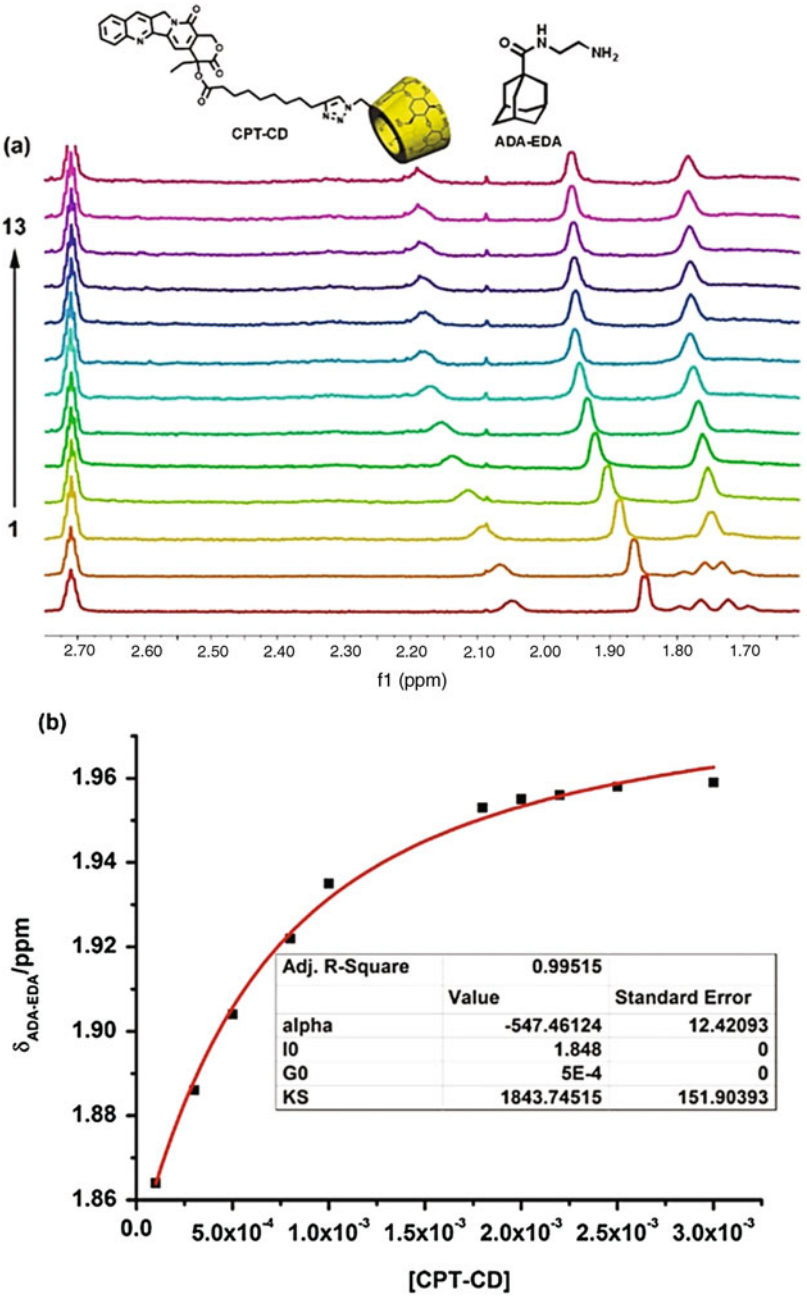

Fig. 15 ^{1}H NMR titration of ADA-EDA with CPT-CD. (a) ^{1}H NMR spectra of ADA-EDA (0.5 mM) upon the addition of 0, 0.1, 0.3, 0.5, 0.8, 1.0, 1.2, 1.5, 1.8, 2.0, 2.2, 2.5, and 3.0 mM CPT-CD (spectrum 1 to 13) in D_2O containing 3% DMSO-d^6 at 25 °C. (b) Nonlinear least-squares fit of the chemical-shift changes of the ADA-EDA with the initial concentration of CPT-CD. Structures of ADA-EDA and CPT-CD as shown on top Ref. [54]

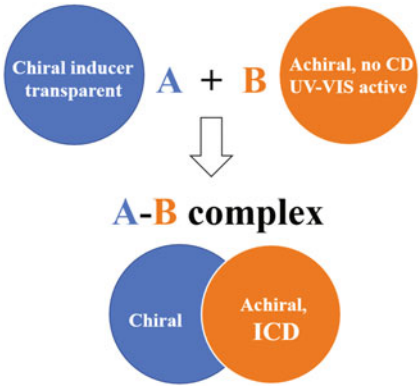

Fig. 16 Simplified representation of generation of ICD

host gives positive ICD while that perpendicular to the axis gives negative ICD. (2) When a chromophore is situated outside the cavity of the host, the sign of ICD becomes reversed to that inside. (3) The magnitude of the ICD signal is greater when the movement of the guest inside the host is hindered.

The application of the rules will be explained through the ICD studies of 2,3-dimethyl naphthalenedicarboxylate (23DMN) with 2-hydroxypropyl-α-, $-\beta$-, and -γ-cyclodextrins (HPCDs) in aqueous solution [61]. As shown in Fig. 17a, 23DMN do not have any CD signal itself, but it can be induced ICD signals in the presence of α-, β-, and γ-HPCD. The ICD spectra for 23DMN:β-HPCD and 23DMN:γ-HPCyD systems exhibit a positive peak around 240 nm, which is corresponding to ^1B_b band of 23DMN. It indicates that 23DMN penetrates inside the cavities of β- and γ-HPCD with its ^1B_b transition parallel to the axis of HPCDs (Fig. 17b). The higher magnitude of the ICD for the 23DMN:β-HPCD suggests a better size-fit and less movement freedom of 23DMN within β-HPCD than γ-HPCD. This host-guest geometry is further confirmed by the molecular mechanics calculations (Fig. 17c). In contrast, the 23DMN with α-HPCD shows a weak negative peak for its ^1B_b band. For the relatively small size of α-HPCD, the 23DMN can not penetrates inside with its ^1B_b transition perpendicular to the axis of α-HPCD. Based on Kodaka's rules, it should be that the 23DMN has most of its chromophore part situated outside the cavity of the α-HPCD (Fig. 17b). In addition, the calculation of the binding constant of host-guest complexes also can be performed by using the ICD technique [62]. From the ICD intensity change of the intensity of the 23DMN upon β-HPCD addition (Fig. 17d), the binding constant, as (910 $\pm$ 50) M^{-1}, can be fitted out by a nonlinear equation for a 1:1 complex (Eq. 13).

41.5 Dynamic Study in Supramolecular Chemistry

One crucial feature of supramolecular system is its dynamic characteristics [63]. The intermolecular interactions between the chemical components in the systems are noncovalent and relatively weak compared to the covalent bond in the molecular

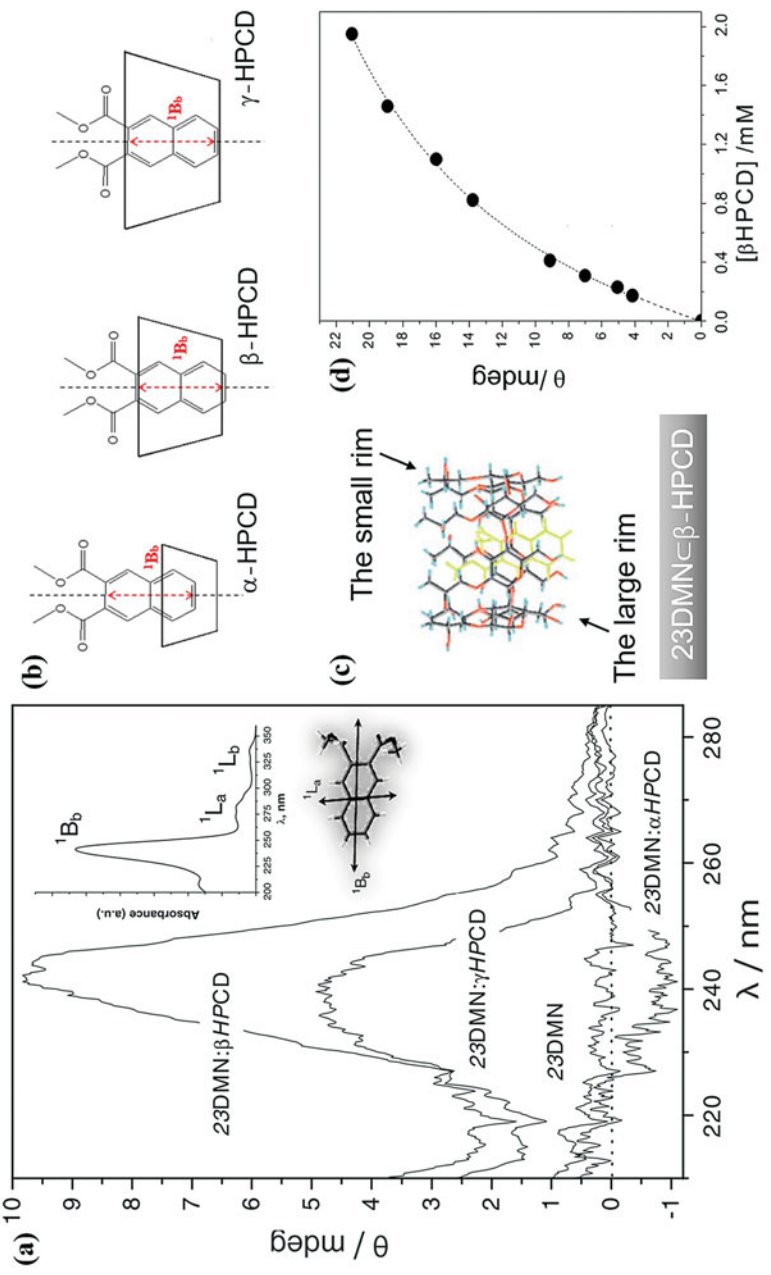

Fig. 17 (**a**) CD spectra of 23DMN and 23DMN in the presence of *α*-, *β*-, and *γ*-HPCD water solutions. Absorption spectrum for a 23DMN water solution and the orientations of the absorption transition moments of 23DMN are shown in the inset. (**b**) Schematic structures of the 23DMN complex with HPCDs. (**c**) Minima binding energy conformation structure for the 23DMN complex with *β*-HPCD by the molecular mechanics calculations. (**d**) Nonlinear least-squares fit of the ellipticity values with the initial concentration of *β*-HPCD for the 23DMN/*β*-HPCD system Refs. [61, 62]

systems. Therefore, the chemical components in supramolecular systems associate and dissociate with each other reversibly. As written by Jean-Marie Lehn, "indeed, supramolecular chemistry is intrinsically a dynamic chemistry in view of the lability of the non-covalent interactions connecting the molecular components of a supramolecular entity." [64] The dynamic of supramolecular system might be crucial to the application scenarios. For example, a drug delivery system might require the release of drugs in the timescale of hours [65], while a dye stabilizing system might require the release of dyes in the timescale of days or even months [18]. However, the information provided by dynamic studies cannot be inferred from thermodynamic studies or structural studies. For example, the trend for the rate of complexation process can be opposite from that for the stability of the complex [66]. In contrast, the information provided by the dynamic study can be employed to infer or explain the results from the thermodynamic study and the structural study.

The dynamic study in the supramolecular chemistry has not been developed to the same extent as the thermodynamic study or the molecular structural design. This situation may be due to fact that the complexity and the diversity of the supramolecular systems limit the equipment and the technique that can be employed. For example, the dissociation of complex can proceed very fast (e.g., within 0.1 μs for the β-cyclodextrin-xanthone complex [67]) or very slow (e.g., >27 h for the CB[7]-1,1′-bis(trimethylammoniomethyl)ferrocene complex [68]). The slow dynamic process (e.g., equilibrating on a timescale longer than minutes) is convenient to be studied by the techniques aforementioned in this chapter, e.g., steady-state fluorescence and absorbance spectroscopies or NMR. During data collection for the supramolecular system, the concentration of the species can be approximately treated as being constant because the time of determination is too short for the process to proceed (known as psudoequilibrium state). Thus, the data points collected at each sampling time can be used to study supramolecular dynamics. In contrast, the fast process cannot be studied by those techniques because the process equilibrates within the determination time and no dynamics information can be obtained. To study the fast process, some relaxation techniques were developed [69].

In 1950s, Manfred Eigen developed a method of "kinetic relaxation" (or known as "chemical relaxation") to study very fast reactions, e.g., the neutralization process of hydronium ion and hydroxide ion [70, 71]. In brief, the methodology of chemical relaxation studies includes perturbing a system at equilibrium, recording the relaxation process (i.e., the process for the system to re-achieve the equilibrium) as the kinetic trace, and analyzing the kinetic trace. The binding mechanism for the supramolecular system and the related association and dissociation rate constants for the relevant reactions in the system are determined during the analyzing process. The perturbation process, which must be faster than the relaxation process, can be achieved by changing temperature (i.e., "temperature jump"), changing pressure (i.e., "pressure jump"), changing the concentration of supramolecular components (i.e., "stopped flow") or changing the energy state of the chemical species (e.g., generating significant amount of excited state of species by the laser flash photolysis experiments (Fig. 18) [72].

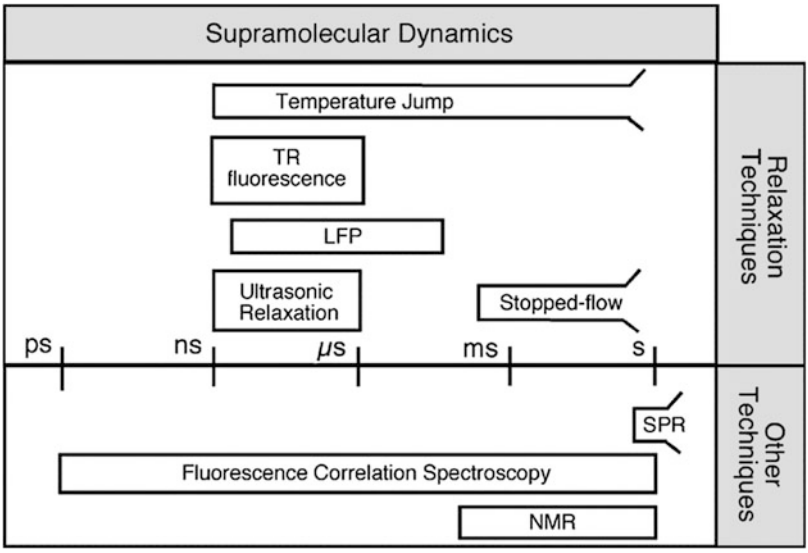

Fig. 18 Techniques suitable for the supramolecular dynamics study at different timescales Ref. [69]

In general, the binding process between the guest and the host molecules proceeds by two steps: (i) the formation of intermediates driven by the host-guest recognition according to the surface properties of the guest and the host molecules (i.e., an exclusion complex), and (ii) the formation of the final host-guest complexes whose geometry and structural distribution depend on the dynamic properties of the complex (i.e., an inclusion complex) [73]. Whether the exclusion complex is detectable or not is different, case by case. For example, the guests with different charge states could associate with cucurbit[6]uril (CB[6]) by different mechanisms: Charged guests with large size bind to CB[6] by forming exclusion complexes firstly and then inclusion complexes, whereas neutral guests with similar sizes move into the cavity of CB[6] directly without the formation of detectable exclusion complexes [13].

For a simple system with two supramolecular components, the binding process could be very fast and equilibrate within 1 millisecond, e.g., the association rate constant for binding of some guests to cyclodextrins and cucurbit[7]uril could be within the range of 4×10^8 M^{-1} s^{-1} –10^9 M^{-1} s^{-1} [10, 74]. With the increase of complexity of supramolecular assemblies, the assembling process dramatically slows down from a sub-millisecond timescale to a millisecond or longer timescale [23, 75]. It is worth noting that some picosecond and femtosecond studies have been conducted for the supramolecular systems [76]. In these cases, the time window of the measurement is too short for the association and dissociation between guest and host cavities. Rather, the ultrafast dynamic studies examined the effect of the host cavities on the vibrational relaxation process of the tripped guests.

41.6 Conclusion

Overall, this chapter introduces four basic and common spectroscopies, i.e., absorbance, fluorescence, NMR, and ICD spectroscopies and their applications in supramolecular chemistry. These spectroscopies are profusely and successfully used in structural, thermodynamic and dynamic studies of supramolecular systems. Absorbance, fluorescence and classic 1D NMR spectroscopies are useful tools to monitor the formation of host-guest assemblies with the binding mechanism and the binding affinity being determined. 2D NMR techniques are convenient ways to reveal the intermolecular interactions as well as the position of guest within the host cavity. ICD experiments are often performed for supramolecular conformation characterization. And with the dynamic methodologies at different timescales, the characteristics of the dynamic process in supramolecular systems and the binding mechanism could be clarified. Moreover, the basic principles in the experimental design and practical operation of spectroscopic experiments were introduced in detailed with specified examples. This knowledge is very important to make the experimental design and data collection rightly especially for beginners. In all, the comprehensive and rational use of these methods and techniques will help us to obtain more complete and accurate insights in supramolecular chemistry.

Acknowledgments We thank National Natural Science Foundation of China (21502059), Natural Science Foundation of Guangdong Province, China (2018A0303130007), and Fundamental Research Funds for the Central Universities, China (2018MS38).

References

1. James TD (2017) Specialty grand challenges in supramolecular chemistry. Front Chem 5:83
2. Liu K, Kang Y, Wang Z, Zhang X (2013) 25th anniversary article: reversible and adaptive functional supramolecular materials: “noncovalent interaction” matters. Adv Mater 25(39): 5530–5548
3. Dsouza RN, Pischel U, Nau WM (2011) Fluorescent dyes and their supramolecular host/guest complexes with macrocycles in aqueous solution. Chem Rev 111(12):7941–7980
4. Elbashir AA, Aboul-Enein HY (2015) Supramolecular analytical application of cucurbit[n]urils using fluorescence spectroscopy. Crit Rev Anal Chem 45(1):52–61
5. Schneider HJ, Hacket F, Rudiger V, Ikeda H (1998) NMR studies of Cyclodextrins and Cyclodextrin complexes. Chem Rev 98(5):1755–1786
6. Pastor A, Martínez-Viviente E (2008) NMR spectroscopy in coordination supramolecular chemistry: a unique and powerful methodology. Coord Chem Rev 252(21–22):2314–2345
7. Allenmark S (2003) Induced circular dichroism by chiral molecular interaction. Chirality 15(5):409–422
8. Cui W, Wang L, Xu L, Zhang G, Meier H, Tang H, Cao D (2018) Fluorescent-cavity host: an efficient probe to study supramolecular recognition mechanisms. J Phys Chem Lett 9(5): 1047–1052
9. Nishijima M, Wada T, Mori T, Pace TCS, Bohne C, Inoue Y (2007) Highly enantiomeric supramolecular [4 + 4] Photocyclodimerization of 2-Anthracenecarboxylate mediated by human serum albumin. J Am Chem Soc 129(12):3478–3479
10. Tang H, Fuentealba D, Ko YH, Selvapalam N, Kim K, Bohne C (2011) Guest binding dynamics with cucurbit[7]uril in the presence of cations. J Am Chem Soc 133(50):20623–20633

11. Schonbeck C, Li H, Han BH, Laursen BW (2015) Solvent effects and driving forces in Pillararene inclusion complexes. J Phys Chem B 119(22):6711–6720
12. Cheng W, Tang H, Wang R, Wang L, Meier H, Cao D (2016) Selective precipitation of alkyl dihalides using a newly synthesized water-soluble bisphosphorylpillar[5]arene. Chem Commun 52(52):8075–8078
13. Marquez C, Nau WM (2001) Two mechanisms of slow host-guest complexation between cucurbit[6]uril and cyclohexylmethylamine: pH-responsive supramolecular kinetics. Angew Chem Int Ed 40(17):3155–3160
14. Hoffmann R, Knoche W, Fenn C, Buschmann H-J (1994) Host-guest complexes of cucurbituril with the 4-methylbenzylammonium ion, alkali-metal cations and NH4+. J Chem Soc Faraday Trans 90(11):1507–1511
15. Marquez C, Hudgins RR, Nau WM (2004) Mechanism of host-guest complexation by Cucurbituril. J Am Chem Soc 126(18):5806–5816
16. Neugebauer R, Knoche W (1998) Host-guest complexes of cucurbituril with 4-amino-4′-nitroazobenzene and 4,4′-diaminoazobenzene in acidic aqueous solutions. J Chem Soc, Perk Trans 2(3):529–534
17. Thomas SS, Tang H, Bohne C (2019) Noninnocent role of Na+ ions in the binding of the N-Phenyl-2-naphthylammonium cation as a Ditopic guest with cucurbit[7]uril. J Am Chem Soc 141:9645
18. Mohanty J, Nau WM (2005) Ultrastable rhodamine with cucurbituril. Angew Chem Int Ed 44(24):3750–3754
19. Dorrance RC, Hunter TF (1977) Absorption and emission studies of solubilization in micelles. Part 4. – studies on cationic micelles with added electrolyte and on lecithin vesicles: excimer formation and the Ham effect. J Chem Soc Faraday Trans 73(0):1891
20. Ham JS (1953) A new electronic state in benzene. J Chem Phys 21(4):756–758
21. Dong DC, Winnik MA (1982) THE Py SCALE OF SOLVENT POLARITIES. SOLVENT EFFECTS ON THE VIBRONIC FINE STRUCTURE OF PYRENE FLUORESCENCE and EMPIRICAL CORRELATIONS WITH ET and Y VALUES. Photochem Photobiol 35 (1):17–21
22. Dong DC, Winnik MA (1984) The Py scale of solvent polarities. Can J Chem 62(11): 2560–2565
23. Tang H, de Oliveira CS, Sonntag G, Gibb CLD, Gibb BC, Bohne C (2012) Dynamics of a supramolecular capsule assembly with pyrene. J Am Chem Soc 134(12):5544–5547
24. Porel M, Jayaraj N, Kaanumalle LS, Maddipatla MVSN, Parthasarathy A, Ramamurthy V (2009) Cavitand Octa acid forms a nonpolar Capsuleplex dependent on the molecular size and hydrophobicity of the guest. Langmuir 25(6):3473–3481
25. De FS, van SJ, Boens N, De SFC (1996) On the use of dynamic fluorescence measurements to determine equilibrium and kinetic constants. The inclusion of pyrene in β-cyclodextrin cavities. Chem Phys Lett 249(1–2):46–52
26. Luo J, Xie Z, Lam JW, Cheng L, Chen H, Qiu C, Kwok HS, Zhan X, Liu Y, Zhu D, Tang BZ (2001) Aggregation-induced emission of 1-methyl-1,2,3,4,5-pentaphenylsilole. Chem Commun 1(18):1740–1741
27. An BK, Kwon SK, Jung SD, Park SY (2002) Enhanced emission and its switching in fluorescent organic nanoparticles. J Am Chem Soc 124(48):14410–14415
28. Feng G, Kwok RTK, Tang BZ, Liu B (2017) Functionality and versatility of aggregation-induced emission luminogens. Appl Phys Rev 4(2):021307
29. Zhang M, Yin S, Zhang J, Zhou Z, Saha ML, Lu C, Stang PJ (2017) Metallacycle-cored supramolecular assemblies with tunable fluorescence including white-light emission. Proc Natl Acad Sci USA 114(12):3044–3049
30. Yan X, Wang M, Cook TR, Zhang M, Saha ML, Zhou Z, Li X, Huang F, Stang PJ (2016) Light-emitting superstructures with anion effect: coordination-driven self-assembly of pure Tetraphenylethylene Metallacycles and Metallacages. J Am Chem Soc 138(13):4580–4588
31. Jiang M, Gu X, Kwok RTK, Li Y, Sung HHY, Zheng X, Zhang Y, Lam JWY, Williams ID, Huang X, Wong KS, Tang BZ (2018) Multifunctional AIEgens: ready synthesis, tunable

emission, Mechanochromism, mitochondrial, and bacterial imaging. Adv Funct Mater 28(1): 1704589
32. Hong Y, Lam JWY, Tang BZ (2011) Aggregation-induced emission. Chem Soc Rev 40(11): 5361–5388
33. Xu L, Wang R, Cui W, Wang L, Meier H, Tang H, Cao D (2018) Stronger host-guest binding does not necessarily give brighter particles: a case study on polymeric AIEE-tunable and size-tunable supraspheres. Chem Commun 54(67):9274–9277
34. Zhu Y, Xu L, Wang L, Tang H, Cao D (2019) Effect of scaffold structures on the artificial light-harvesting systems: a case study with an AIEE-active pillar[5]arene dyad. Chem Commun 55(42):5910–5913
35. Ma X, Wang J, Tian H (2019) Assembling-induced emission: an efficient approach for amorphous metal-free organic emitting materials with room-temperature phosphorescence. Acc Chem Res 52(3):738–748
36. Lou X-Y, Yang Y-W (2018) Manipulating aggregation-induced emission with supramolecular macrocycles. Adv Opt Mater 6(22):1800668
37. Yi S, Kaifer AE (2011) Determination of the purity of cucurbit[n]uril (n = 7, 8) host samples. J Org Chem 76(24):10275–10278
38. Turro NJ, Ramamurthy V, Scaiano JC (2009) Principles of molecular photochemistry: an introduction. University Science Books, Sausalito
39. Mohanty J, Nau WM (2004) Refractive index effects on the oscillator strength and radiative decay rate of 2,3-diazabicyclo[2.2.2]oct-2-ene. Photochem Photobiol Sci 3(11–12):1026–1031
40. Tang H, Sutherland AS, Osusky LM, Li Y, Holzwarth JF, Bohne C (2014) Chiral recognition for the complexation dynamics of beta-cyclodextrin with the enantiomers of 2-naphthyl-1-ethanol. Photochem Photobiol Sci 13(2):358–369
41. Renny JS, Tomasevich LL, Tallmadge EH, Collum DB (2013) Method of continuous variations: applications of job plots to the study of molecular associations in organometallic chemistry. Angew Chem Int Ed 52(46):11998–12013
42. Benesi HA, Hildebrand JH (1949) A spectrophotometric investigation of the interaction of iodine with aromatic hydrocarbons. J Am Chem Soc 71(8):2703–2707
43. Zhang W, Zhang YM, Li SH, Cui YL, Yu J, Liu Y (2016) Tunable Nanosupramolecular aggregates mediated by host-guest complexation. Angew Chem Int Ed Engl 55(38):11452–11456
44. Silverstein RM, Webster FX, Kiemle D (2005) Spectrometric identification of organic compounds. Wiley, Hoboken
45. Wu H, Chen Y, Zhang L, Anamimoghadam O, Shen D, Liu Z, Cai K, Pezzato C, Stern CL, Liu Y, Stoddart JF (2019) A dynamic Tetracationic macrocycle exhibiting Photoswitchable molecular encapsulation. J Am Chem Soc 141(3):1280–1289
46. Kassem S, van Leeuwen T, Lubbe AS, Wilson MR, Feringa BL, Leigh DA (2017) Artificial molecular motors. Chem Soc Rev 46(9):2592–2621
47. Cui JS, Ba QK, Ke H, Valkonen A, Rissanen K, Jiang W (2018) Directional shuttling of a stimuli-responsive cone-like macrocycle on a single-state symmetric dumbbell axle. Angew Chem Int Ed Engl 57(26):7809–7814
48. Claridge TDW (1999) High resolution NMR techniques in organic chemistry. Pergamon, Oxford
49. Yang ZX, Chen Y, Liu Y (2008) Inclusion complexes of bisphenol a with cyclomaltoheptaose (beta-cyclodextrin): solubilization and structure. Carbohydr Res 343 (14):2439–2442
50. Zhu H, Liu J, Shi B, Wang H, Mao Z, Shan T, Huang F (2018) Pillararene-based host–guest recognition facilitated magnetic separation and enrichment of cell membrane proteins. Mater Chem Front 2(8):1475–1480
51. Price WS (1997) Pulsed-field gradient nuclear magnetic resonance as a tool for studying translational diffusion: part 1. Basic theory. Concepts Magn Reson 9(5):299–336
52. Johnson CS Jr (1999) Diffusion ordered nuclear magnetic resonance spectroscopy: principles and applications. Prog Nucl Magn Reson Spectrosc 34(3–4):203–256

53. Evan-Salem T, Cohen Y (2007) Octahydroxypyridine[4]arene self-assembles spontaneously to form hexameric capsules and dimeric aggregates. Chem Eur J 13(27):7659–7663
54. Yang Y, Zhang YM, Li D, Sun HL, Fan HX, Liu Y (2016) Camptothecin-polysaccharide co-assembly and its controlled release. Bioconjug Chem 27(12):2834–2838
55. Berova N, Nakanishi K, Woody RW, Woody R (2000) Circular dichroism: principles and applications. Wiley-VCH, New York
56. Gawronski J, Grajewski J (2003) The significance of induced circular dichroism. Org Lett 5(18):3301–3303
57. Krois D, Brinker UH (2006) Circular dichroism of cyclodextrin complexes. Wiley-VCH, Weinheim
58. Kodaka M (1991) Sign of circular dichroism induced by .beta.-cyclodextrin. J Phys Chem 95(6):2110–2112
59. Kodaka M (1993) A general rule for circular dichroism induced by a chiral macrocycle. J Am Chem Soc 115(9):3702–3705
60. Kodaka M (1998) Application of a general rule to induced circular dichroism of naphthalene derivatives complexed with Cyclodextrins. Chem A Eur J 102(42):8101–8103
61. Usero R, Alvariza C, Gonzalez-Alvarez MJ, Mendicuti F (2008) Complexation of dimethyl 2,3-naphthalenedicarboxylate with 2-hydroxypropyl-alpha-, -beta- and -gamma-cyclodextrins in aqueous solution by fluorescence, circular dichroism and molecular mechanics. J Fluoresc 18(6):1103–1114
62. Mendicuti F, González-Álvarez MJ (2010) Supramolecular chemistry: induced circular dichroism to study host−guest geometry. J Chem Educ 87(9):965–968
63. Lehn J-M (1988) Supramolecular chemistry – scope and perspectives molecules, Supermolecules, and molecular devices (Nobel lecture). Angew Chem Int Ed Engl 27(1):89–112
64. Lehn JM (2007) From supramolecular chemistry towards constitutional dynamic chemistry and adaptive chemistry. Chem Soc Rev 36(2):151–160
65. Webber MJ, Langer R (2017) Drug delivery by supramolecular design. Chem Soc Rev 46(21):6600–6620
66. Jiang W, Ajami D, Rebek J (2012) Alkane lengths determine encapsulation rates and equilibria. J Am Chem Soc 134(19):8070–8073
67. Liao Y, Frank J, Holzwarth JF, Bohne C (1995) Effect of excitation on the host-guest equilibrium constants of cyclodextrin complexes. J Chem Soc Chem Commun (2):199–200
68. Rekharsky MV, Mori T, Yang C, Ko YH, Selvapalam N, Kim H, Sobransingh D, Kaifer AE, Liu S, Isaacs L, Chen W, Moghaddam S, Gilson MK, Kim K, Inoue Y (2007) A synthetic host-guest system achieves avidin-biotin affinity by overcoming enthalpy-entropy compensation. Proc Natl Acad Sci USA 104(52):20737–20742
69. Pace TCS, Bohne C (2007) Dynamics of guest binding to supramolecular systems: techniques and selected examples. Adv Phys Org Chem 42:167–223
70. Eigen M (1972) Immeasurably fast reactions. In: Nobel lectures in chemistry (1963–1970). Elsevier, Amsterdam, pp 170–203
71. Eigen M (1954) Methods for investigation of ionic reactions in aqueous solutions with half-times as short as 10–9 sec. Application to neutralization and hydrolysis reactions. Discuss Faraday Soc 17:194–205
72. Bernasconi CF (1976) Relaxation kinetics. Academic, New York
73. Koehler G, Grabner G, Klein CTH, Marconi G, Mayer B, Monti S, Recthaler K, Rotkiewicz K, Veirnstein H, Wolschann P (1996) Structure and spectroscopic properties of cyclodextrin inclusion complexes. J Incl Phenom Mol Recognit Chem 25(1–3):103–108
74. Bohne C (2006) Supramolecular dynamics studied using photophysics. Langmuir 22(22): 9100–9111
75. Peng S, Barba-Bon A, Pan Y-C, Nau WM, Guo D-S, Hennig A (2017) Phosphorylation-responsive membrane transport of peptides. Angew Chem Int Ed 56(49):15742–15745
76. Douhal A (2004) Ultrafast guest dynamics in Cyclodextrin Nanocavities. Chem Rev 104(4): 1955–1976